VILNIUS TECH
Vilnius Gediminas Technical University

Journal of Environmental Engineering and Landscape Management
ISSN 1648–6897 / eISSN 1822-4199
2023 Volume 31 Issue 1: 52–66
https://doi.org/10.3846/jeelm.2023.18482

ASSESSMENT OF SPATIAL AND TEMPORAL DISTRIBUTION OF URBAN HEAT ISLANDS (UHI) IN SEMI-ARID CLIMATE

Nidal M. HUSSEIN[1], Mohammed N. ASSAF[2*]

[1]*Department of Civil Engineering, University of Petra, Amman, Jordan*
[2]*Department of Civil Engineering & Architecture, University of Pavia, Pavia, Italy*

Received 08 February 2022; accepted 09 November 2022

Highlights

- Spatio-temporal analysis of LST was executed for the years from 2000 to 2019 for Amman, Jordan.
- The relationship of LST with vegetation indicators (NDVI and EVI) is diurnal dependent.
- Identified UHI intensity of range 2.4 °C to 2.87 °C (1.00–1.95 °C) for daytime (nighttime).
- Vegetation lands dropped daytime and nighttime LST.
- Average temperature was positively correlated with UHI intensity.
- The average wind speed was significantly adversely correlated with UHI intensity.

Abstract. An urban heat island phenomenon has increased in the last decades due to rapid urbanization, resulting in a significant impact on local climate. In this study, remote sensing data was used to analyze Spatiotemporal patterns of Urban Heat Island Intensity (UHII) over a 20 years period in a semi-arid climate area. The relationship between the Land Surface Temperature (LST), vegetation and Land Cover Types (LCTs) were examined. The relation between the UHII and its driving factors (different LCTs and meteorological conditions) was analyzed. Analysis of 8-day daytime and nighttime LST data acquired from MODerate-resolution Imaging Spectroradiometer (MODIS) shows that Amman has a significant UHII in both daytime and night time. The results show a negative correlation between the LST and vegetation indicators and between the UHII and the wind speed average, indicating a positive correlation between the UHII and temperature. Vegetation has been proven to significantly reduce LST, mainly in the daytime, due to its cooling effect that results from the transpiration process and shadow effect.

Keywords: Urban Heat Island, Land Cover Type, land surface temperature, vegetation indexes, spatio-temporal pattern, MODIS.

Introduction

The world has experienced a high rate of urbanization in the last decades; the urban area has extended by 1.6 times between 2001 and 2018, while Africa and Asia have shown the highest growth rates (Huang et al., 2021). As a result, metropolis areas and their residents have become one of the fundamental drivers of environmental change because of a substantial accumulation of human-created impervious areas (Ejiagha et al., 2020). Moreover, the expansion rate is expected to increase due to better socioeconomic opportunities in the coming years. Therefore, in order to provide enough accommodation to cover this high rate of expansion, natural surfaces (wetlands, water bodies, agricultural land, forested land) are being altered to impervious/built-up areas (Zhao et al., 2020). This alteration in the composition and configuration of land uses led to a wide range of environmental effects such as food security, climate change, and biodiversity loss (Ejiagha et al., 2022; Yohannes et al., 2021; Faridatul et al., 2022). Even though these effects can differ according to the scale of the investigation, they are considerably detectable within local environments (Grimm et al., 2008).

The accelerated urbanization has significantly carried a change in energy balance, natural cycling, water sources distribution, natural drainage networks, natural

*Corresponding author. E-mail: *ma.mohammed.assaf@gmail.com*

topography, temperature, precipitation, biodiversity and associated environmental problems that have affected the quality of life (Cheng et al., 2008; Chen et al., 2017; Assaf, 2019). Urban Heat Island (UHI), which was first described in 1818, is a terminology to describe the difference in temperature between the urbanized area, which is hotter and the surrounding non-urbanized area (Oke & Hannell, 1970). This phenomenon can be related to the artificial surface's lower albedo or surface reflectivity compared to the adjacent natural surface (Ejiagha et al., 2020).

Dark artificial surface has a high capacity to absorb incoming solar radiation and reflect again to the surroundings, consequently increasing air temperature. UHI has an impact similar to global warming despite the difference in causes and spatial extension. UHI, like global warming, can raise energy consumption, directly and indirectly affecting human livability and ecosystem services (Abdullah et al., 2022; U.S. Environmental Protection Agency, 2008). Therefore, treating the UHI issue can be considered climate change adaptation and mitigation solutions to reach sustainable development goals (United Nations & Department of Economic and Social Affairs, 2015). Also, UHI is associated with urban water, air pollution, human health and energy management (U.S. Environmental Protection Agency, 2008). So monitoring the urban island of cities is a significant issue that is addressed to study its environmental change and climate variability, especially in Jordan. Jordan is a developing country with limited natural resources, particularly water and energy, a high population growth rate and a massive influx of refugees (Abdelal et al., 2022; Hussein et al., 2022). These factors give urban expansion and their influences, like Urban Heat Island (UHI), significant importance.

UHI can be measured through the air temperature or land surface temperature (LST) (United Nations & Department of Economic and Social Affairs, 2015). The air temperature data is acquired from an automatic and conventional weather station with a high temporal resolution and a low spatial resolution (Oke, 1976). However, the LST can be easily obtained through thermal infrared (TIR) remote sensing data with the advantage of high spatial distribution and low temporal resolution (Imhoff et al., 2010).

Remote sensing technology has shown an ability to characterize urban environment materials and retrieve land surface features (Hussein et al., 2021; Hussein & Assaf, 2020). Thus, remote sensing data has the ability to enhance the realization of the UHI phenomenon and its effects. Moreover, various investigations have addressed the UHI utilizing LST retrievals (Rhinane et al., 2012; Sobrino et al., 2012; Botje et al., 2022; Dewan et al., 2021a).

Although UHI's significant impacts on the environment, human well-being, and policymakers' decisions, there is a lack of studying the UHI in Jordan. Several researches were carried out to study the urban expansion in some cities in Jordan. Remote sensing and geographic information systems techniques (GIS) have been integrated to show urban expansion and evaluate its environmental and socioeconomic impacts (Rawashdeh & Saleh, 2006; Saleh & Al Rawashdeh, 2007). Also, some studies have estimated and analyzed the urban growth and sprawl in Jordan (Oroud & Al-Rousan, 2004; Ghurah et al., 2018; Alnsour, 2016). All of these studies did not address the UHI issues in their investigation.

Recently, the urbanization process's effects on food supply and irrigation demands were studied in Jordan. Indeed, Simulation models were used to analyze various spatial-temporal scenarios of urbanization on cropland demand and irrigation water requirements by taking into consideration the changes in socio-economy and climate (Koch et al., 2018).

In contrast, UHI topics have a broad interest in a global range; Several studies have been done in a different variety of cities, such as tropical cities (Estoque et al., 2017), coastal cities (Sakakibara & Owa, 2005), and desert cities (Bokaie et al., 2016).

Understanding the driving factors of UHI is a crucial issue to mitigate its effect and provide the decision-makers and urban planners with the vital information to distribute the land cove types appropriately to help dissipate the heat. The most significant UHI driving factors were found to be land cover types, anthropogenic heat sources, the size of the urban area and meteorological conditions (Peng et al., 2012; Coseo & Larsen, 2014; Debbage & Shepherd, 2015; Guo et al., 2015; Tan & Li, 2015). Those factors have been studied widely (Nichol, 2005; Grimm et al., 2008; Lemonsu et al., 2015). However, most former studies focused on individual variable examination (Du et al., 2016). Also, they focus on daytime analysis, which leads to significant gaps in addressing the diurnal variation (Zhou et al., 2019). Therefore, more research analysis is needed to identify the UHI driving factors considering the diurnal variation.

The study primarily investigates spatial-temporal variations in LST during daytime and nighttime in Amman, Jordan. Moreover, the relationship between UHI intensity and influencing factors (different LCTs and meteorological conditions) is examined.

1. Materials and methods

1.1. Study area

Amman is the capital and the largest city of Jordan. Amman is located in the west-central part of the country (Figure 1), within latitudes 31°57′ N and longitudes 35°56′ E. Amman is the most populous metropolitan city in Jordan, with a dramatic population increase from 2,353,300 in 2004 to 4,430,700 in 2019 (Department of Statistics, 2019). It encompasses a total area of around 1,680 km^2. It is characteristic of diverse topography where its elevation ranges between 700 m to 1100 m. Amman has a semi-arid climate, classified under BSh (Arid Steppe Hot) according to Köppen climate classification (Carver et al., 2002). The study area faces four seasons in a year:

- Summer season from June to August (hot during day time with a mean maximum temperature of around 32 °C).

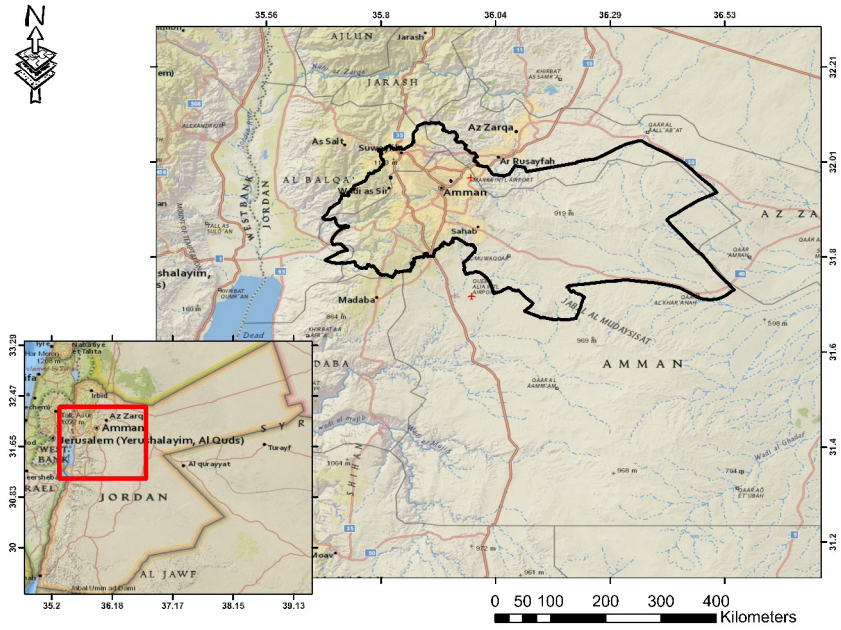

Figure 1. Map of the study area, Amman, Jordan

– Autumn season from September to October (with broad vacillations in mean air temperature due to atmospheric conditions).
– Winter season from November to February (cold nights with the average minimum temperature reaching 5 °C).
– Spring season from March to May (with moderate air temperature during days and nights).

The mean relative humidity is around 43% in the summer season and elevates up to 71% in the winter season. The rainy season extends from October to March, while the summer season is arid. The average annual precipitation over the study area is about 245 mm.

1.2. Data

Practical investigation of spatial-temporal urban heating needs a sizeable geospatial database over several years. This study uses MODerate-resolution Imaging Spectroradiometer (MODIS) global LST 8-day composite at a 1-km resolution (MYD11A2 products, version 6) from 2001 to 2019 for both nighttime and daytime. MODIS LST data validation with in situ measurements provided an absolute deviation of less than 1 °C (Wan, 2008; Pablos et al., 2016). MODIS global LST product is one of the most broadly utilized LST remote sensing datasets for UHI investigations (Imhoff et al., 2010). Summer is considered an exemplary period for the thermal environment and urban expansion evaluations (Peng et al., 2016; Brazel et al., 2007; Brazel et al., 2000). Therefore, for this study, the analysis is conducted for the summer season (June to August) as Amman has hot, dry and clear weather conditions. The MODIS LST products have a quality flag in the form of a (SDS) layer that provides information on each pixel's quality control (QC). Hence, QC information was used to select only high-quality LST pixels (QC flag value of 0) for the analysis. Twelve MODIS LST images are available during each summer for the chosen time frame. Hence, 228 daytime and nighttime LST images were obtained for the 19 years from 2001 to 2019.

Modis Global Land Cover Type (LCT) data (MCD12Q1, products, version 6) with a spatial resolution of 500 m was used to extract yearly land cover data of the study area. The MCD12Q1 classifies the land cover properties using the International Geosphere Biosphere Programme (IGBP) scheme, including 17 classes. Normalized difference vegetation index (NDVI) and enhanced vegetation index (EVI) obtained from MOD13A3 data (monthly composite), with 1000 m spatial resolution, were used to distinguish green belts from 2001 to 2019. In addition, pixels with high-grade quality flags data were selected. To diminish the elevation influences on the UHII, the Global Digital Elevation Model (GDEM) data derived from the Advanced Spaceborne Thermal Emission and Reflection Radiometer (ASTER) was used to obtain the elevation of the study area pixels. Table 1 presents the remote sensing data used for the research.

Table 1. Remote sensing data used in this research

Data	Source	Sensor	Temporal resolution	Spatial resolution (m)
LST	MODIS (MOD11A2)	MODIS	8 day	1000
LCT	MODIS (MCD12Q1)	MODIS	Yearly	500
NDVI	MODIS (MOD13A1)	MODIS	Monthly	1000
EVI	MODIS (MOD13A1)	MODIS	Monthly	1000
GDEM	ASTGTM	ASTER	–	30

1.3. Method

Preparing the study data set for analysis included pre-processing of remote sensing data. The pre-processing stage includes re-projected and reformatting MODIS data. The MCD12Q1 and GDEM data were resampled to 1000 m to preserve consistency with LST data spatial resolution. The pre-processing of remote sensing data has been performed using ArcMap 10.6 software.

Defining urban and rural areas boundaries was performed based on several steps. Firstly, the urban area boundary has been acquired by extracting land area from MCD12Q1 data of 2010 based on IGBP classification. Secondly, to identify the rural area, a buffer polygon, away from the urban boundary, has been created. The distance of the buffer has been selected to ensure that the size of the rural area is roughly the same as the urban area. The rural buffer was 10 km away from the existing urban boundary. Finally, to reach an accurate and fair comparison between urban and the surrounding rural areas, the area classified as water bodies or its elevation falls without the range of the urban area's mean elevation of the urban area ±50 m are excluded from the rural area (Zhou et al., 2016; Yao et al., 2018a, 2018b).

The study area pixels are extracted from the MODIS LST images for both daytime and nighttime. Then pixel values are converted to LST in Kelven by multiplying it with the scale factor; then, it was converted to Celsius. The mean LST images of the study area are then computed by averaging twelve summer LST images for every year, resulting in 19 daytime and 19 nighttime images. The LST values for both urban and rural areas were extracted for each year from 2001 to 2019. Then the UHI intensity (UHII) was calculated for each year as the difference in mean LST between urban and rural areas. The UHII can be determined using Equation (1) (Oke & East, 1971; Oke, 1973).

$$\text{UHI intensity (°C)} = T_{\text{urban average}} - T_{\text{rural average}}. \quad (1)$$

NDVI and EVI have been used to extract vegetation greenness information over the study area. NDVI and EVI for the study area pixels are extracted from MOD13A1 data, and pixel values are converted to NDVI and EVI by multiplying them with the scale factor. Overall, we considered 57 images for each NDVI and EVI (three images during each summer from 2001–2019). The mean NDVI and EVI images are then calculated by averaging the three summer images yearly, resulting in 19 NDVI and 19 EVI mean images.

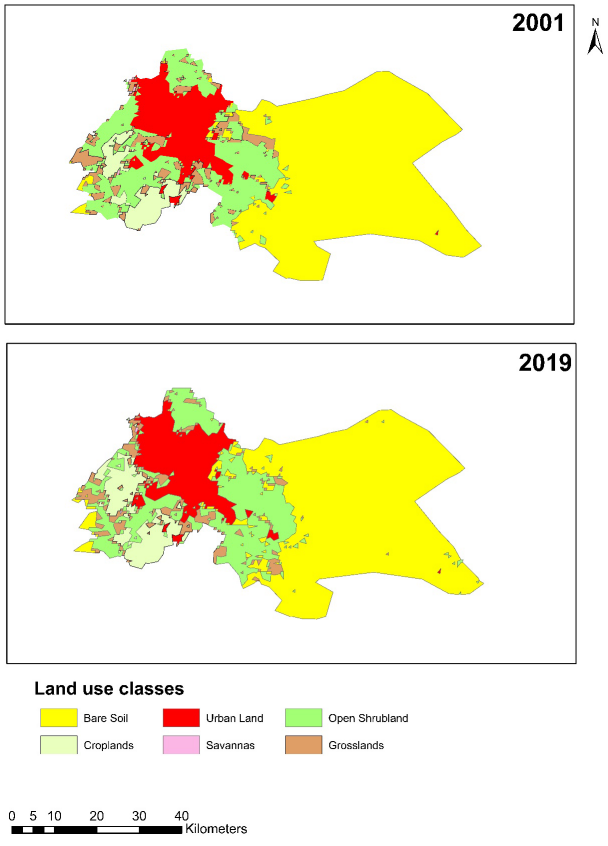

Figure 2. LULC map of Amman of 2001 and 2019

2. Results and discussions

2.1. LCT pattern of Amman city

The spatial distribution of LCT within the study area in 2001 and 2019 is presented in Figure 2. The bare soil is represented the predominant type in the study area, where it covers approximately half of area's landscape. Urban areas are concentrated in the northwest of the city; it is noted that there are few green spaces or any other cover types within the urban areas. In general, there are neither water bodies nor wetland areas within Amman city. The vegetation lands are located around the urban areas, especially in the north and southeast, while the croplands and grasslands are scattered in a random manner representing various pieces in the study area. In 2019, there appears to be an increase in vegetation lands over bare soil in the central regions. However, there is also an increase in cropland/gross lands over the vegetation lands in the west and southwest. Besides, there appears to be a slight increase in urban areas. The spatial extent of built-up cover over the study area does not change that much; however, the urban expansion in Amman took a vertical pattern more than a horizontal one, and the urban intensity was dramatically increased. In the last twenty years, almost all of the open areas and pervious lands inside the city have been turned into buildings.

2.2. LST distribution during day and night times

The LST distributions over Amman city are described in Figures 3 and 4 for the day and the night times, respectively. For the daytime, the LST is ranged between 37–51 °C, while during nighttime, the range is decreased to 18–29 °C.

2.2.1. Daytime

The LST over the urban in 2001 is ranging between 40.0–47.0 °C. In 2006, 2011, and 2015, the LST ranges over the urban area were decreased to 37.9–45.1 °C, 38.2–45.3 °C,

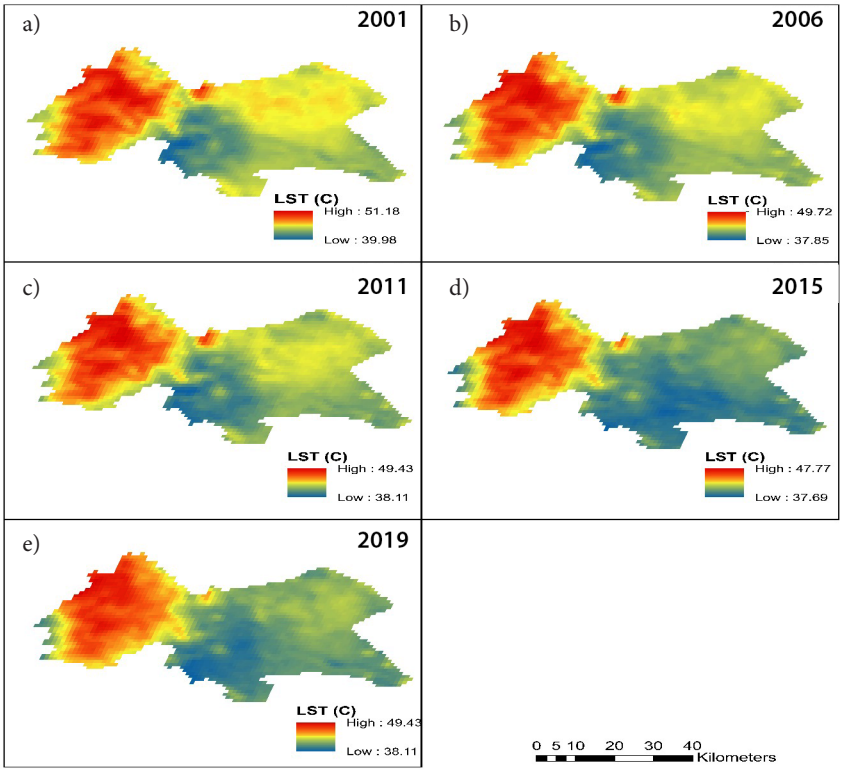

Figure 3. Daytime Land Surface Temperature (LST) distributions for Amman city: a) 2011, b) 2006, c) 2011, d) 2015, and e) 2019

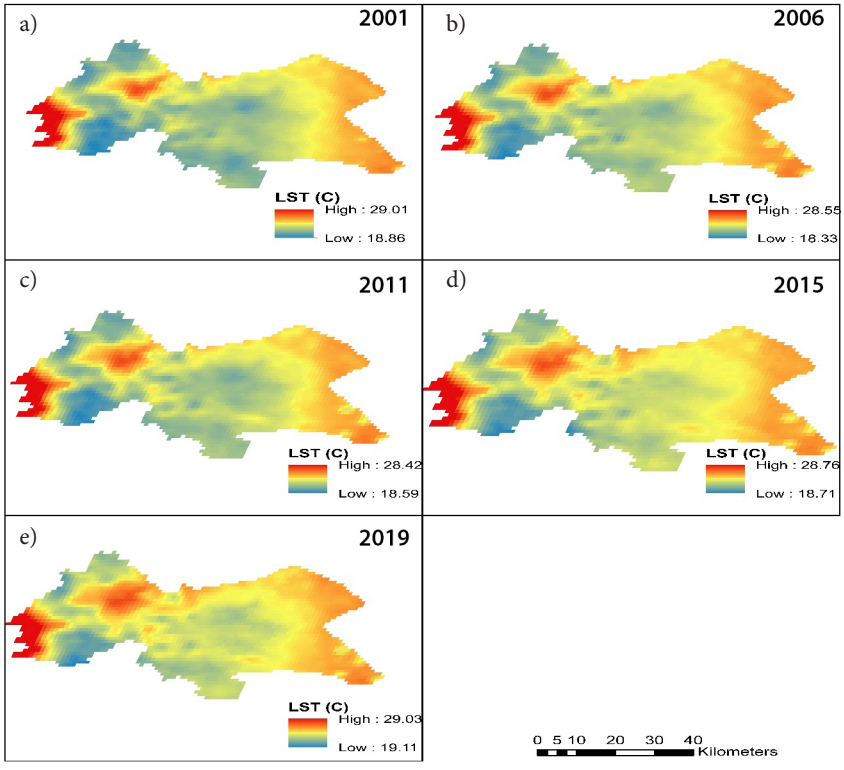

Figure 4. Nighttime Land Surface Temperature (LST) distributions for Amman city: a) 2011, b) 2006, c) 2011, d) 2015, and e) 2019

and 37.7–44.8 °C, respectively. During the year 2019, the urban area's LST range increased to 38.2–46.4 °C. The LST over the bare soil ranges between 46.9–51.1 °C, 46.5–49.7 °C, and 46.2–49.4 °C in 2001, 2006, and 2011, respectively. In 2015 and 2019, the LST ranges for bare soil are noticed as 45.2–47.7 °C and 45.4–49.4 °C, respectively. The LST over the open shrubland, croplands, and grasslands areas is in the range of 41.5–49.1 °C and 41.1–48.7 °C for 2000 and 2004, respectively. For the years 2008, 2013, and 2017 those areas are found to possess LST in the range 38.9–47.0 °C, 38.1–46.7 °C, and 39.4–47.2 °C, respectively.

2.2.2. Nighttime

The urban area over the city region has the LST ranges of 20.1–28.1 °C, 20.0–28.4 °C, and 19.9–27.8 °C, for the years 2001, 2006, and 2011, respectively. In the years 2015 and 2019, the LST ranges are found to be slightly decreased to 19.4–27.1 °C and 19.3–27.3 °C for the urban area. The temperature ranges for bare soil areas during the years 2001, 2006, and 2011 are 24.2–29.0 °C, 23.9–28.5 °C, and 24.1–28.2 °C, respectively. In 2015 and 2019, the temperature ranges over the bare soil are 23.1–28.7 °C and 22.7–29.0 °C, respectively. The LST over the open shrubland, croplands, and grasslands areas during 2001, 2006, 2011, 2015, and 2019 are observed in the wide range of 18.0–29.0 °C; where southwest of Amman that close to Jordan valley has a hot spot area with a ring between 27.0–29.0 °C, whereas the other areas have a ring of 18.0–23.0 °C.

2.3. Mean LST trend for different times

The temporal mean LST variations in urban and rural areas are shown in Figure 5. In both cases, the Average LST in the urban area is higher than in the rural area. For urban and rural areas, the average LST shows a rising trend over the study period. UHII during the nighttime was more strong comparing with the daytime.

Average LSTs during daytime and nighttime vary from 43.51–45.71 °C and 20.46–23.25 °C, respectively, for urban areas. Likewise, for rural areas, average LSTs during daytime and nighttime range from 41.10–43.17 °C and 18.76–21.75 °C, respectively. Average LSTs during daytime and nighttime are 44.81 °C and 21.96 °C, respectively, for urban areas and 42.13 °C and 20.49 °C, respectively, for rural areas. So it's clear that daytime has observed a considerable variation between urban and rural LSTs than nighttime.

2.4. UHI intensity pattern

Figure 6 gives the average UHI intensity (variation in mean LST between the urban and rural areas) during each year of the study period. The positive value of the UHI intensity difference indicates a clear existence of UHII during daytime and nighttime as the LST spatial decreased from urban to rural areas. Therefore, the urban area experienced a higher temperature than the surrounding rural area. The average intensity during daytime ranges from 2.41 °C to 2.87 °C, with an average UHI intensity of 2.67 °C. The average intensity during nighttime ranges from 1.00 °C to 1.95 °C, with an average UHI intensity of 1.47 °C. UHII has been found tougher during the daytime than nighttime. The average UHI intensity of the investigated studied area for the whole time (day and night) has been found to be 2.07 °C.

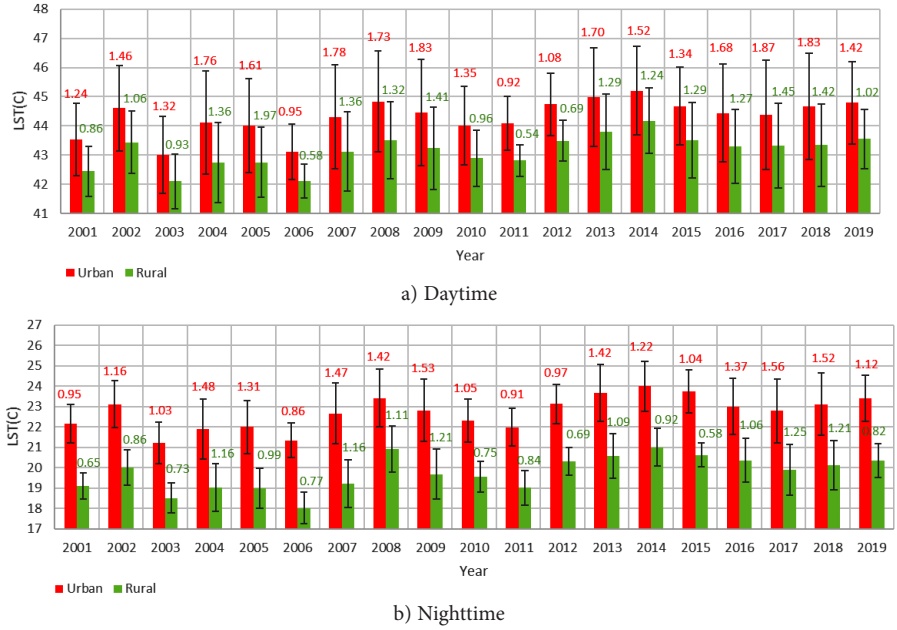

a) Daytime

b) Nighttime

Note: The error bars represent the standard deviation of the mean LST, while the number at the top of the bars represent the pooled standard deviation of LST.

Figure 5. Bar charts showing the temporal variation of average LST in urban and rural areas: a) daytime and b) nighttime

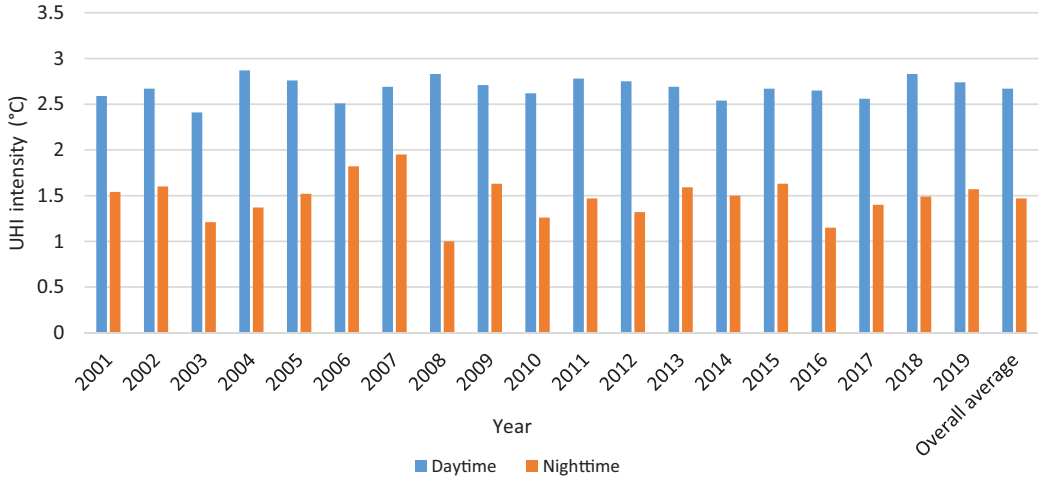

Figure 6. Average UHI intensity (°C) during daytime and nighttime

2.5. Vegtation indices pattern

Vegetation spatial and temporal patterns have been analyzed using NDVI and EVI indicators over the study area shown in Figures 7 and 8, respectively. The low value of vegetation indicators (NDVI and EVI) indicates poorly vegetated intensity over the study area, while vegetated areas have a high value. Considering the color legend of Figures 7 and 8, the intensity vegetation area appears blue while the poor vegetation area looks brown. The urban area has slight blue spots, the center shows much dark brown and with the direction to the outskirts, the color becomes light brown. The rural area shows different intensity blue spots and higher NDVI values, comparing with the urban area. This can be attributed to urbanization, which reduces the scope for green cover growth. Figure 8 shows a similar tendency in EVI spatial distribution. EVI values are ordinarily lesser than the NDVI values as a result of reform in EVI computations. The statistical parameters (min, max, mean and standard deviation) of NDVI and EVI are shown in Tables 2 and 3, respectively.

Table 2. Statistics of NDVI over the study area

NDVI	Min	Max	Mean	Standard deviation
2001	0.069	0.394	0.161	0.0354
2006	0.072	0.414	0.166	0.0386
2011	0.074	0.387	0.167	0.0372
2015	0.080	0.428	0.193	0.0408
2019	0.071	0.432	0.183	0.0477

Table 3. Statistics of EVI over the study area

EVI	Min	Max	Mean	Standard deviation
2001	0.057	0.313	0.128	0.0217
2006	0.058	0.327	0.141	0.0260
2011	0.059	0.322	0.142	0.0251
2015	0.057	0.333	0.142	0.0260
2019	0.058	0.340	0.141	0.0315

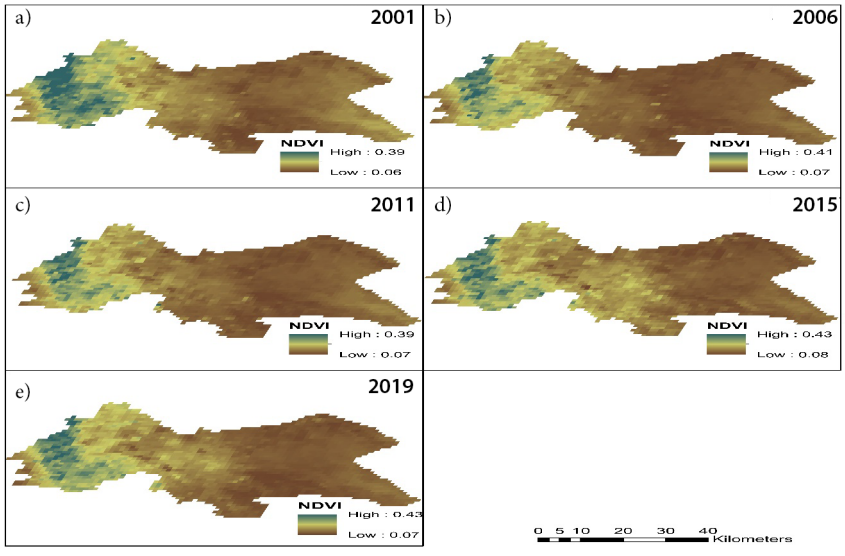

Figure 7. Spatial distributions of NDVI for Amman city: a) 2001, b) 2006, c) 2011, d) 2015, and e) 2019

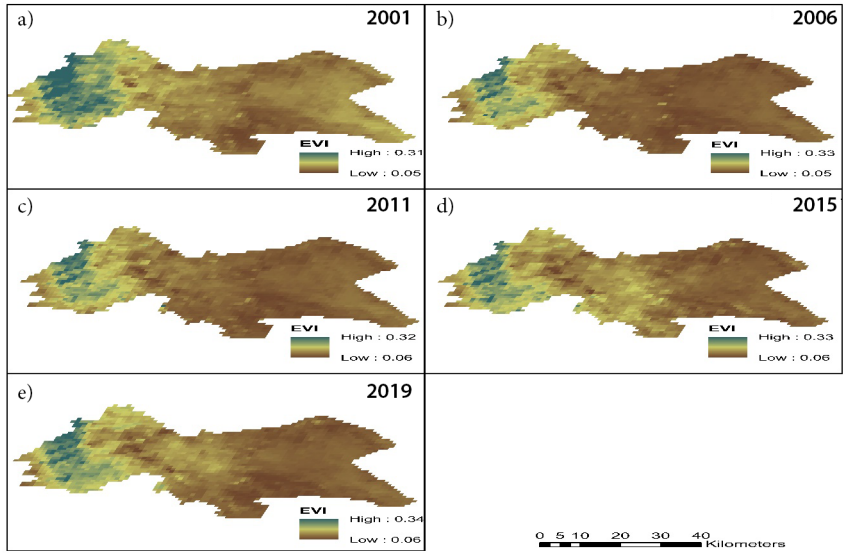

Figure 8. Spatial distributions of EVI for Amman city: a) 2001, b) 2006, c) 2011, d) 2015, and e) 2019

2.6. Relationship between LST and vegetation indicators (VIs)

To recognize the interrelationship between the surface temperature and vegetation cover, the LST, NDVI and EVI were plotted against each other. Stratified random sampling method was used to select the sample points using the LCTs as strata. In total, 150 samples point were chosen and the corresponding LST, NDVI and EVI values were taken for daytime and nighttime of each year. The stratified random sampling helps analyze the correspondence relationship coefficient according to various categories.

Figure 9 shows the relationship between mean LST and VIs for daytime and nighttime of 2001 and 2019. The trend lines in these figures indicate an inverse correlation between LST and VIs.

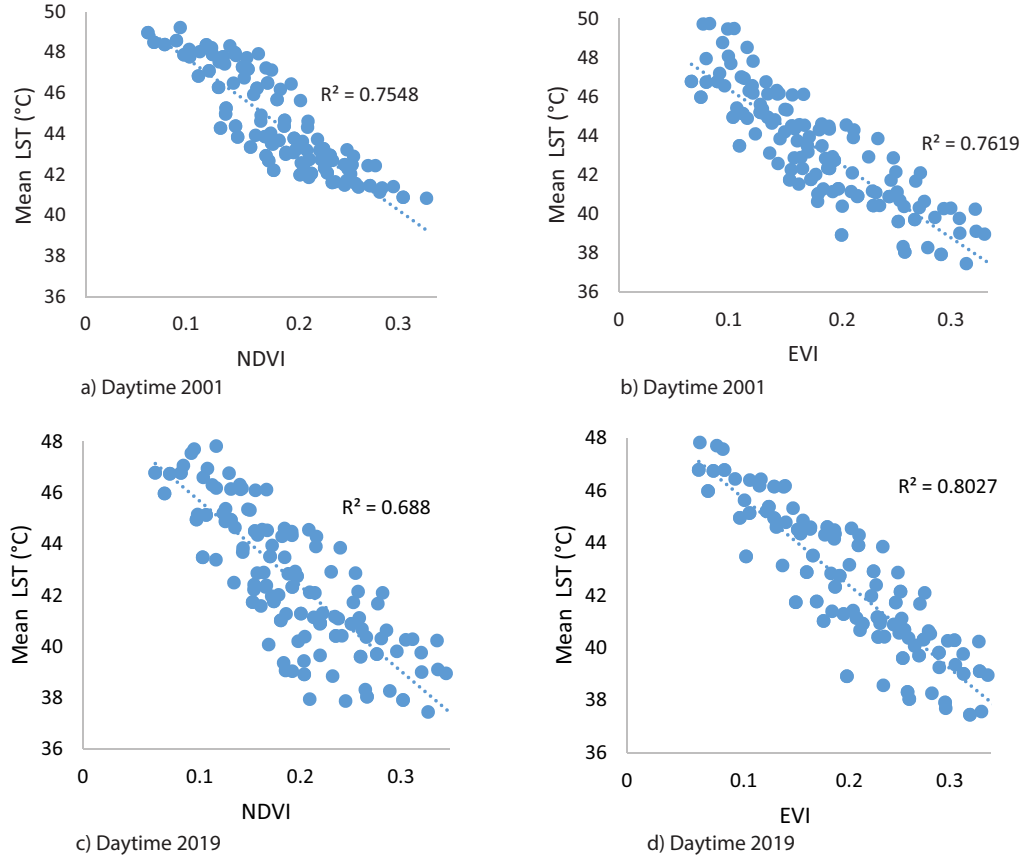

Figure 9. *To be continued*

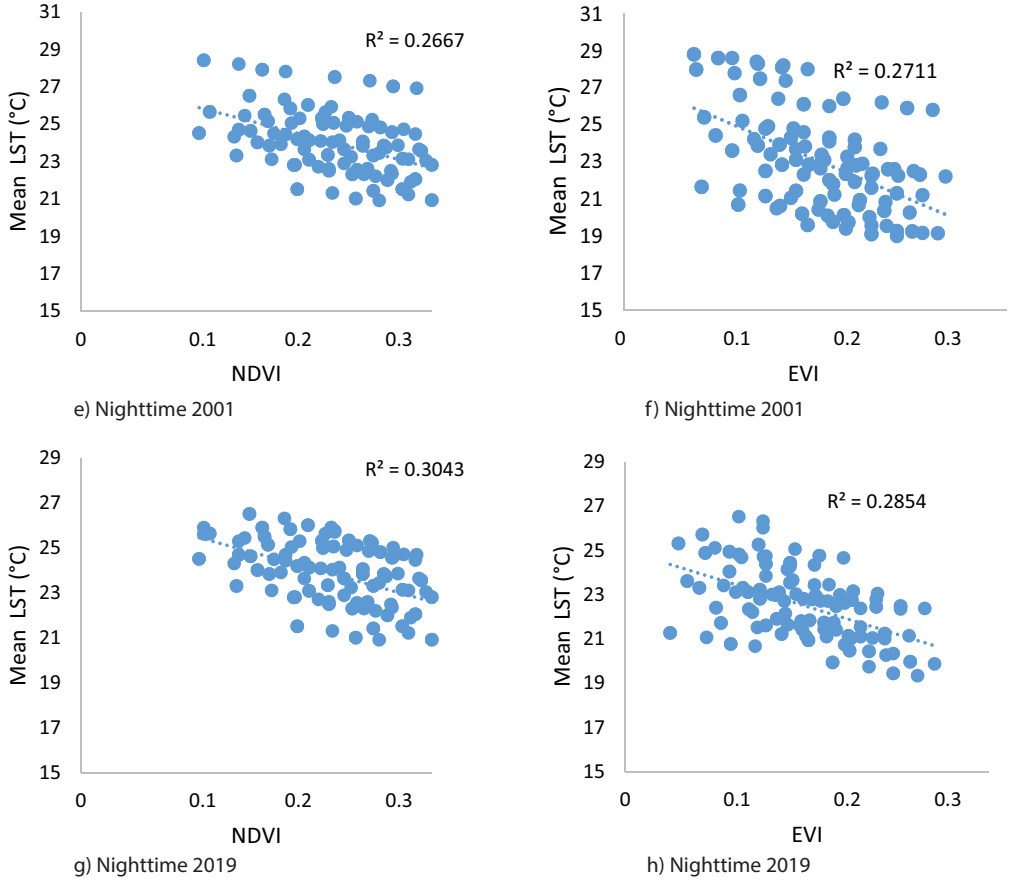

Figure 9. Mean LST and VI relationship for daytime and nighttime od 2011 and 2019

Figure 10 shows the R^2 value of LST-NDVI relationship for the daytime over the study period (2001–2019), the range varies from 0.70 to 0.81 with an average value of 0.75. The R^2 value for nighttime varies from 0.19 to 0.31, with an average value of 0.26. This clearly indicates that the relationship of NDVI with LST fits better for daytime than nighttime.

Figure 11 shows the R^2 value of LST-EVI relationship for the daytime over the study period (2001–2019). The range varies from 0.71 to 0.82, with an average value of 0.78. The R^2 value for nighttime varies from 0.23 to 0.37, with an average value of 0.31.

2.7. Land cover types and LST

Table 4 shows the LSTs distribution in different LCTs classes. The study period was divided into three periods; 2001–2006, 2007–2013, 2014–2019, where the average of LSTs was taken for each period. The LSTs of different LCTs are considerably diversified as a result of variations

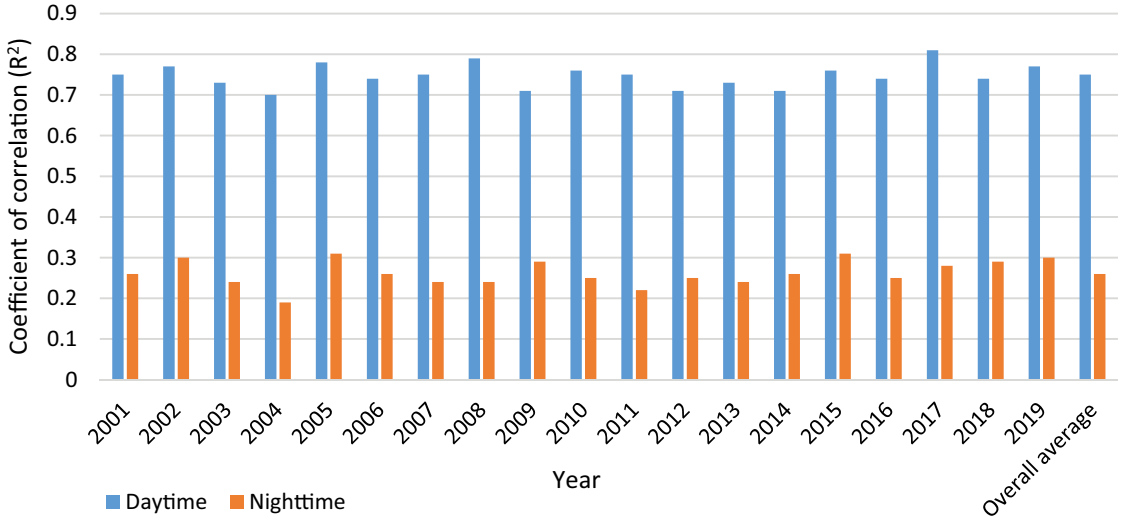

Figure 10. Coefficient of correlation for mean LST and NDVI relationship

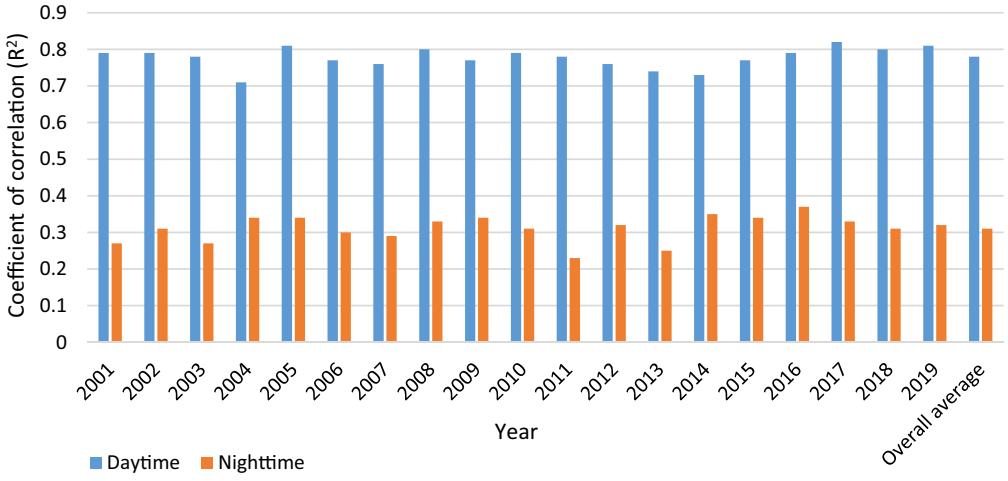

Figure 11. Coefficient of correlation for mean LST and EVI relationship

Table 4. LCTs classes with their LST for periods 2001–2006, 2007–2013 and 2014–2019

LULC Class	2001–2006		2007–2013		2014–2019	
	Daytime	Nighttime	Daytime	Nighttime	Daytime	Nighttime
Bare Soil	43.62	22.83	43.47	22.24	43.34	23.12
Urban Land	44.92	25.67	45.23	26.3	45.81	26.92
Open Shrub land	42.18	22.11	42.66	22.57	42.83	22.89
Cropland	43.61	21.81	43.47	21.37	44.18	22.31
Gross lands	42.93	22.43	42.96	22.14	43.12	22.84

in artificial heat sources and the differences in properties of surface materials' thermal-biological (Su et al., 2010). The urban area has the highest temperature in both daytime and nighttime. While the lowest average temperature is in the green area (open shrubland and gross lands), this indicates the cooling role of vegetation and its impact on decreasing the land temperatures. A fluctuation in the LSTs distribution can be observed in almost all LCTs classes concerning time. For instance, LST values of the green area for the periods 2001–2006, 2007–2013 and 2014–2019 were found to be 42.18 °C, 42.66 °C and 42.83 °C for daytime respectively, and 21.1 °C, 21.57 °C and 21.89 °C, for nighttime respectively. This manifests a continual rise of the LST of that class within the period. While the LST average amounts for Cropland in periods 2001–2006, 2007–2013 and 2014–2019 were found to be 43.61 °C, 43.47 °C and 44.18 °C for daytime respectively, and 220.1 °C, 22.14 °C and 22.84 °C, for nighttime respectively. This apparent vacillation of LST values within the period. Likewise, the vacillation of LST values were also recognized in bare soil areas. The rise in LST value was noted in the urban land as 44.92 °C, 45.23 °C and 45.81 °C for daytime respectively, and 25.67 °C, 26.3 °C and 26.92 °C, for nighttime for the periods 2001–2006, 2007–2013 and 2014–2019, respectively. The continual rise in the urban area coupled with the increase in LST values between 2001–2006, 2007–2013 and 2014–2019 indicate that urbanization impacted the increase in LST values in Amman.

2.8. UHI intensity and meteorological conditions

Figure 12 shows the correlation between average temperature during each year's summer months and the corresponding UHI intensity. A significant positive correlation ($p < 0.001$) has been found between the average temperature and the UHI intensity in both daytime and nighttime.

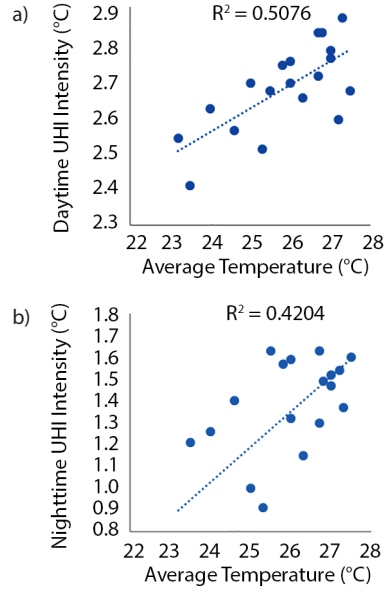

Figure 12. Correlations between UHI intensity and the average temperature of a) daytime and b) nighttime

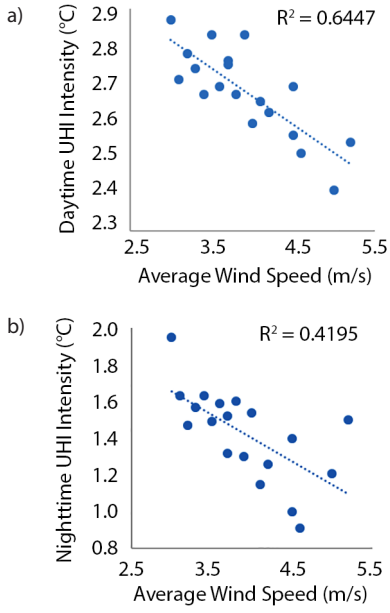

Figure 13. Correlations between UHI intensity and average wind speed: a) daytime and b) nighttime

Figure 13 shows the correlation between average wind speed during each year's summer months and the corresponding UHI intensity. A significant negative correlation ($p < 0.001$) has been found between the average wind speed and the UHI intensity in daytime and nighttime.

3. Discussions

The detected higher daytime UHI intensity compared with the nighttime UHI intensity can be explained by three factors. First, the urban surfaces (pavement materials, building density, building height and building materials) will absorb more radiation and solar energy compared to suburban areas during the day (Strong et al., 2002; Si et al., 2022). Second, the denser buildings and structures in the urban area lead to reduced access to the sky spaces; thus the ground's radiation encounters various reflections between the surfaces and walls in urban areas, resulting in significantly diminished heat loss from the ground to the atmosphere (Kalnay & Cai, 2003). This results in higher LSTs value during the day in the urban areas. Third, cooler transpiration effect of vegetation presence during the daytime contributes to lower LST values. The vegetation cover is denser in the rural areas and leads to an increase in the diurnal differences in the UHI intensity. These outputs are consistent with previous studies findings (Peng et al., 2012; Du et al., 2016; Dewan et al., 2021b; Ejiagha et al., 2022).

An inverse correlation has been detected between LST and VIs indicated (Figure 9). The presence of vegetation cover can provide a cooling effect and reduce the LST mainly due to two reasons; transpiration process and shadow effect. Transpiration raises the latent heat fluxes and moisture availability, which create a cooling effect on the surface temperature (Sharma & Joshi, 2015; Li et al., 2011; Peng et al., 2012; Yuan & Bauer, 2007). The vegetation shadow can reduce the radiation on the nearby surface, thus adjusting the energy interactions on these surfaces and thereby reducing the land temperature (Mathew et al., 2017). A strong and significant negative correlation was found between the LST and VIs during the daytime. This reflects the vital role that vegetation plays to decrease the LSTs and mitigate the UHI intensity in the urban area. Hu and Jia observed that the vegetation fraction declined by 16% from 1990–2007, leading to a 2.5 increasing in the LST in Guangzhou, China (Hu & Jia, 2010). However, the LST and VIs had insignificant correlations during the nighttime; which was anticipated due to the absence of shadow effects and evapotranspiration during the night (Peng et al., 2012; Arnfield, 2003). Moreover, the outputs indicate that the relationship of EVI with LST is better than the LST-NDVI relationship for both daytime and nighttime. EVI provides a better representation for extent vegetation than NDVI and, therefore, the preferable relationship of LST with EVI. The insignificant relationship between the LST and VIs during the nighttime can be attributed to the absence of vegetative transpiration (Zhou et al., 2014; Arnfield, 2003).

The surface materials' solar energy absorption and thermal properties govern the surface heat storage and the land temperature during the daytime (Peng et al., 2012). Therefore, the urban areas with higher absorption capacity and higher emissivity experience higher LSTs (Kjelgren & Montague, 1998). However, Greenlands have less emissivity and thermal conductivity (in the absence of wetlands in this study), so it has a lower temperature during the daytime (Imhoff et al., 2010; Zhao et al., 2020). The latent heat flux from the ground to the sky controls the land temperature during the night (Voogt & Oke, 2003). Vegetation lands have a low temperature due to three factors. Firstly, vegetation land consists of exposed bare soil and sparse vegetation, which releases heat quickly at night due to its low thermal capacity, thus decreasing the temperature (Weng, 2001). Secondly, extensive vegetation areas are also located in almost blank spaces. Accordingly, the long-wave radiation from the surface can be quickly scattered into the air and decrease the land temperature (Chudnovsky et al., 2004). Third, through the transpiration process, plant roots can absorb the moisture from the soil and release it into the air, which reduces the LSTs (Kjelgren & Montague, 1998).

A significant correlation was founded between the UHI intensity and meteorological conditions. The surrounding temperature considerably impacts land surface materials. Urban land surface materials mainly involve pavement, clay and concrete, which have thermal inertia and high heat flux and are affected substantially by surrounding temperatures (Debbage & Shepherd, 2015; Si et al., 2022). While in the suburban area, the vegetation and bare soil are the main constituents of land surface material. They have a low heat flux, therefore less affected by the surrounding temperature than urban land surface materials (Oke, 1973). Slow wind velocities restrict horizontal airflow and enable spatial thermal heterogeneity to

strengthen and continue. In contrast, high wind serves to homogenize and mix adjacent suburban and urban air masses (Schatz & Kucharik, 2014). Therefore, with the increase in wind speed, the temperature difference between the urban and suburban areas will decrease, leading to a decrease in the UHI intensity. The results are consistent with previous studies findings (Du et al., 2016; Estoque et al., 2017; Agarwal & Tandon, 2010).

Studying the UHI effects is a new subject for developing countries like Jordan. Until now, Jordanian government does not have any specific program for UHI mitigation; even it has not added to any climate change adaptation plans. The corresponding procedure development should be initiated by thoroughly investigating the UHI effects and quantifying the potential of each mitigation technique. This research quantified the UHI and investigated its relationship with the driving factors (different LCTs and meteorological conditions). Moreover, this study's outputs would help develop strategies to reduce the UHI effect like increasing the urban tree planting, using the green roofs, urban surface materials and urban configurations that affect wind porosity. This research can open a door for further investigation to quantify the UHI mitigating option, such as street and pavement albedo, urban vegetation planning, urban canopy control and urban building density in the future.

Conclusions

Remote sensing data of LST, LCTs and vegetation indicators have been utilized in the current research to analysis the UHI pattern in Amman, Jordan. The 8-day LST data for both daytime and nighttime has been carried out for the summer months (June, July and August) from 2001 to 2019. Significant UHII has been observed in both daytime and nighttime where the average UHII during daytime ranges from 2.41 °C to 2.87 °C, with an average UHII of 2.67 °C. While the average intensity during nighttime was found to be lower than daytime with ranges from 1.00 °C to 1.95 °C, and an average UHII of 1.47 °C. An inverse proportionality was detected between LST and vegetation indicators (NDVI and EVI). The R^2 between the LST and NDVI was 0.75 and 0.26 on average for daytime and nighttime, respectively. While the R^2 between the LST and EVI was 0.78 and 0.31 on average for daytime and nighttime, respectively. These results indicate the EVI is a better representative of vegetation than NDVI, and the cooling effect of vegetation is more effective during the daytime. Also, the results show that LCT affects the LSTs. Consequently, designers should encourage ecological corridors construction to facilitate energy and mass transfer among urban areas and their adjacent areas. Also, they should focus on establishing and improving the green areas in residential, commercial and industrial buildings.

Vegetation has been proven to significantly reduce LST mainly in the daytime due to its cooling effect that results from the transpiration process and shadow effect. Therefore, increasing the percentage of vegetation in the commercial, residential and industrial sectors is highly recommended, and the decision-makers and urban planners are required to establish policies and regulations to encourage urban developers to consider the impact of their urbanization activities and execute an effective and appropriate mitigation measures.

Acknowledgements

Authors would like to thank the Deanship of Scientific Research and Graduate Studies at University of Petra (grant no. 2/7/2019).

Author contribution

Nidal M. Hussein: conceptualization; methodology; validation; funding acquisition; project administration; supervision; writing – review & editing. Mohammed N. Assaf: conceptualization; methodology; data curation; formal analysis; investigation; visualization; project administration; writing – original draft; writing – review & editing.

Conflicts of interest

The authors declare no conflict of interest. The funding sources for this research had no role in the design; the collection, analyses, or interpretation of data; the writing of the manuscript; or in the decision to publish the results.

References

Abdelal, Q., Assaf, M. N., Al-Rawabdeh, A., Arabasi, S., & Rawashdeh, N. A. (2022). Assessment of Sentinel-2 and Landsat-8 OLI for small-scale inland water quality modeling and monitoring based on handheld hyperspectral ground truthing. *Journal of Sensors*, *2022*, 4643924. https://doi.org/10.1155/2022/4643924

Abdullah, S., Adnan, M. S. G., Barua, D., Murshed, M. M., Kabir, Z., Chowdhury, M. B. H., Hassan, Q. K., & Dewan, A. (2022). Urban green and blue space changes: A spatiotemporal evaluation of impacts on ecosystem service value in Bangladesh. *Ecological Informatics*, *70*, 101730. https://doi.org/10.1016/j.ecoinf.2022.101730

Agarwal, M., & Tandon, A. (2010). Modeling of the urban heat island in the form of mesoscale wind and of its effect on air pollution dispersal. *Applied Mathematical Modelling*, *34*(9), 2520–2530. https://doi.org/10.1016/j.apm.2009.11.016

Alnsour, J. A. (2016). Managing urban growth in the city of Amman, Jordan. *Cities*, *50*, 93–99. https://doi.org/10.1016/j.cities.2015.08.011

Al Rawashdeh, S., & Saleh, B. (2006). Satellite monitoring of urban spatial growth in the amman area, Jordan. *Journal of Urban Planning and Development*, *132*(4), 211–216. https://doi.org/10.1061/(ASCE)0733-9488(2006)132:4(211)

Arnfield, A. J. (2003). Two decades of urban climate research: A review of turbulence, exchanges of energy and water, and the urban heat island. *International Journal of Climatology*, *23*(1), 1–26. https://doi.org/10.1002/joc.859

Assaf, M. N. (2019). *Utilizing Landsat 8 and Sentinel 2 satellites images for water quality evaluation in King Tala Dam*. German Jordanian University.

Bokaie, M., Zarkesh, M. K., Arasteh, P. D., & Hosseini, A. (2016). Assessment of urban heat island based on the relationship between land surface temperature and land use/land cover in Tehran. *Sustainable Cities and Society*, *23*, 94–104. https://doi.org/10.1016/j.scs.2016.03.009

Botje, D., Dewan, A., & Chakraborty, T. C. (2022). Comparing coarse-resolution land surface temperature products over Western Australia. *Remote Sensing*, *14*(10), 2296. https://doi.org/10.3390/rs14102296

Brazel, A., Gober, P., Lee, S.-J., Grossman-Clarke, S., Zehnder, J., Hedquist, B., & Comparri, E. (2007). Determinants of changes in the regional urban heat island in metropolitan Phoenix (Arizona, USA) between 1990 and 2004. *Climate Research*, *33*(2), 171–182. https://doi.org/10.3354/cr033171

Brazel, A., Selover, N., Vose, R., & Heisler, G. (2000). The tale of two climates Baltimore and Phoenix urban LTER sites. *Climate Research*, *15*(2), 123–135. https://doi.org/10.3354/cr015123

Carver, S., Mikkelsen, N., & Woodward, J. (2002). Long-term rates of mass wasting in Mesters Vig, northeast Greenland: Notes on a re-survey. *Permafrost and Periglacial Processes*, *13*(3), 243–249. https://doi.org/10.1002/ppp.421

Chen, Y.-C., Chiu, H.-W., Su, Y.-F., Wu, Y.-C., & Cheng, K.-S. (2017). Does urbanization increase diurnal land surface temperature variation? Evidence and implications. *Landscape and Urban Planning*, *157*, 247–258. https://doi.org/10.1016/j.landurbplan.2016.06.014

Cheng, K.-S., Su, Y.-F., Kuo, F.-T., Hung, W.-C., & Chiang, J.-L. (2008). Assessing the effect of landcover changes on air temperature using remote sensing images—A pilot study in northern Taiwan. *Landscape and Urban Planning*, *85*(2), 85–96. https://doi.org/10.1016/j.landurbplan.2007.09.014

Chudnovsky, A., Ben-Dor, E., & Saaroni, H. (2004). Diurnal thermal behavior of selected urban objects using remote sensing measurements. *Energy and Buildings*, *36*(11), 1063–1074. https://doi.org/10.1016/j.enbuild.2004.01.052

Coseo, P., & Larsen, L. (2014). How factors of land use/land cover, building configuration, and adjacent heat sources and sinks explain Urban Heat Islands in Chicago. *Landscape and Urban Planning*, *125*, 117–129. https://doi.org/10.1016/j.landurbplan.2014.02.019

Debbage, N., & Shepherd, J. M. (2015). The urban heat island effect and city contiguity. *Computers, Environment and Urban Systems*, *54*, 181–194. https://doi.org/10.1016/j.compenvurbsys.2015.08.002

Department of Statistics. (2019). *Population of Jordan Kingdom.* Department of Statistics, Jordan Kingdom. http://dosweb.dos.gov.jo/DataBank/JordanInFigures/Jorinfo_2019.pdf

Dewan, A., Kiselev, G., & Botje, D. (2021a). Diurnal and seasonal trends and associated determinants of surface urban heat islands in large Bangladesh cities. *Applied Geography*, *135*, 102533. https://doi.org/10.1016/j.apgeog.2021.102533

Dewan, A., Kiselev, G., & Botje, D., Mahmud, G. I., Bhuian, M. H., & Hassan, Q. K. (2021b). Surface urban heat island intensity in five major cities of Bangladesh: Patterns, drivers and trends. *Sustainable Cities and Society*, *71*, 102926. https://doi.org/10.1016/j.scs.2021.102926

Du, H., Wang, D., Wang, Y., Zhao, X., Qin, F., Jiang, H., & Cai, Y. (2016). Influences of land cover types, meteorological conditions, anthropogenic heat and urban area on surface urban heat island in the Yangtze River Delta Urban Agglomeration. *Science of the Total Environment*, *571*, 461–470. https://doi.org/10.1016/j.scitotenv.2016.07.012

Ejiagha, I. R., Ahmed, M. R., Dewan, A., Gupta, A., Rangelova, E., & Hassan, Q. K. (2022). Urban warming of the two most populated cities in the Canadian Province of Alberta, and its influencing factors. *Sensors*, *22*(8), 2894. https://doi.org/10.3390/s22082894

Ejiagha, I. R., Ahmed, M. R., Hassan, Q. K., Dewan, A., Gupta, A., & Rangelova, E. (2020). Use of remote sensing in comprehending the influence of urban landscape's composition and configuration on land surface temperature at neighbourhood scale. *Remote Sensing*, *12*(15), 2508. https://doi.org/10.3390/rs12152508

Estoque, R. C., Murayama, Y., & Myint, S. W. (2017). Effects of landscape composition and pattern on land surface temperature: An urban heat island study in the megacities of Southeast Asia. *Science of the Total Environment*, *577*, 349–359. https://doi.org/10.1016/j.scitotenv.2016.10.195

Faridatul, M. I., Adnan, M. S. G., & Dewan, A. (2022). Nexus of urbanization and changes in agricultural land in Bangladesh. In K. P. Vadrevu, T. Le Toan, S. S. Ray, & C. Justice (Eds.), *Remote sensing of agriculture and land cover/land use changes in South and Southeast Asian countries* (pp. 455–469). Springer International Publishing. https://doi.org/10.1007/978-3-030-92365-5_26

Ghurah, M. H. A., Kamarudin, M. K. A., Wahab, N. A., Juahir, H., Lananan, F., Maulud, K. A. N. N., & Zin, M. S. M. (2018). Assessment of urban growth and sprawl using GIS and remote sensing techniques in South Ghor region, Al-Karak, Jordan. *International Journal of Engineering & Technology*, *7*(3.14), 5–11. https://doi.org/10.14419/ijet.v7i3.14.16853

Grimm, N. B., Faeth, S. H., Golubiewski, N. E., Redman, C. L., Wu, J., Bai, X., & Briggs, J. M. (2008). Global change and the ecology of cities. *Science*, *319*(5864), 756–760. https://doi.org/10.1126/science.1150195

Guo, G., Wu, Z., Xiao, R., Chen, Y., Liu, X., & Zhang, X. (2015). Impacts of urban biophysical composition on land surface temperature in urban heat island clusters. *Landscape and Urban Planning*, *135*, 1–10. https://doi.org/10.1016/j.landurbplan.2014.11.007

Hu, Y., & Jia, G. (2010). Influence of land use change on urban heat island derived from multi-sensor data. *International Journal of Climatology*, *30*(9), 1382–1395. https://doi.org/10.1002/joc.1984

Huang, X., Huang, J., Wen, D., & Li, J. (2021). An updated MODIS global urban extent product (MGUP) from 2001 to 2018 based on an automated mapping approach. *International Journal of Applied Earth Observation and Geoinformation*, *95*, 102255. https://doi.org/10.1016/j.jag.2020.102255

Hussein, N. M., & Assaf, M. N. (2020). Multispectral remote sensing utilization for monitoring chlorophyll-a levels in inland water bodies in Jordan. *The Scientific World Journal*, *2020*, 1–14. https://doi.org/10.1155/2020/5060969

Hussein, N. M., Assaf, M. N., & Abohussein, S. S. (2021). *Application of sentinel 2 to evaluate colored dissolved organic matter algorithms for inland water bodies in Jordan* [Conference presentation]. Proceedings of the 9th Jordan International Chemical Engineering Conference (JICHEC9).

Hussein, N. M., Assaf, M. N., & Abohussein, S. S. (2022). Sentinel 2 analysis of turbidity retrieval models in inland water bodies: The case study of Jordanian dams. *The Canadian Journal of Chemical Engineering*, 1–14. https://doi.org/10.1002/cjce.24526

Imhoff, M. L., Zhang, P., Wolfe, R. E., & Bounoua, L. (2010). Remote sensing of the urban heat island effect across biomes in the continental USA. *Remote Sensing of Environment*, *114*(3), 504–513. https://doi.org/10.1016/j.rse.2009.10.008

Kalnay, E., & Cai, M. (2003). Impact of urbanization and land-use change on climate. *Nature*, *423*(6939), 528–531. https://doi.org/10.1038/nature01675

Kjelgren, R., & Montague, T. (1998). Urban tree transpiration over turf and asphalt surfaces. *Atmospheric Environment*, *32*(1), 35–41. https://doi.org/10.1016/S1352-2310(97)00177-5

Koch, J., Wimmer, F., & Schaldach, R. (2018). Analyzing the relationship between urbanization, food supply and demand, and irrigation requirements in Jordan. *Science of the Total Environment*, *636*, 1500–1509. https://doi.org/10.1016/j.scitotenv.2018.04.058

Lemonsu, A., Viguie, V., Daniel, M., & Masson, V. (2015). Vulnerability to heat waves: Impact of urban expansion scenarios on urban heat island and heat stress in Paris (France). *Urban Climate*, *14*, 586–605. https://doi.org/10.1016/j.uclim.2015.10.007

Li, J., Song, C., Cao, L., Zhu, F., Meng, X., & Wu, J. (2011). Impacts of landscape structure on surface urban heat islands: A case study of Shanghai, China. *Remote Sensing of Environment*, *115*(12), 3249–3263. https://doi.org/10.1016/j.rse.2011.07.008

Mathew, A., Khandelwal, S., & Kaul, N. (2017). Investigating spatial and seasonal variations of urban heat island effect over Jaipur city and its relationship with vegetation, urbanization and elevation parameters. *Sustainable Cities and Society*, *35*, 157–177. https://doi.org/10.1016/j.scs.2017.07.013

Nichol, J. (2005). Remote sensing of urban heat islands by day and night. *Photogrammetric Engineering Remote Sensing*, *71*(5), 613–621. https://doi.org/10.14358/PERS.71.5.613

Oke, T. R. (1973). City size and the urban heat island. *Atmospheric Environment*, *7*(8), 769–779. https://doi.org/10.1016/0004-6981(73)90140-6

Oke, T. R. (1976). The distinction between canopy and boundary-layer urban heat islands. *Atmosphere*, *14*(4), 268–277. https://doi.org/10.1080/00046973.1976.9648422

Oke, T. R., & East, C. (1971). The urban boundary layer in Montreal. *Boundary-Layer Meteorology*, *1*(4), 411–437. https://doi.org/10.1007/BF00184781

Oke, T. R., & Hannell, F. G. (1970). *The form of the urban heat island in Hamilton, Canada* (Technical Note No. 108). WMO.

Oroud, I., & Al-Rousan, N. (2004). Urban encroachment on rain-fed agricultural lands in Jordan during the second half of the 20th century. *The Arab World Geographer*, *7*(3), 165–180.

Pablos, M., Martínez-Fernández, J., Piles, M., Sánchez, N., Vall-llossera, M., & Camps, A. (2016). Multi-temporal evaluation of soil moisture and land surface temperature dynamics using in situ and satellite observations. *Remote Sensing*, *8*(7), 587. https://doi.org/10.3390/rs8070587

Peng, J., Xie, P., Liu, Y., & Ma, J. (2016). Urban thermal environment dynamics and associated landscape pattern factors: A case study in the Beijing metropolitan region. *Remote Sensing of Environment*, *173*, 145–155. https://doi.org/10.1016/j.rse.2015.11.027

Peng, S., Piao, S., Ciais, P., Friedlingstein, P., Ottle, C., Bréon, F. M., Nan, H., Zhou, L., & Myneni, R. B. (2012). Surface urban heat island across 419 global big cities. *Environmental Science & Technology*, *46*(2), 696–703. https://doi.org/10.1021/es2030438

Rhinane, H., Hilali, A., Bahi, H., & Berrada, A. (2012). Contribution of landsat TM data for the detection of urban heat islands areas case of Casablanca. *Journal of Geographic Information System*, *4*(1), 20–26.

Sakakibara, Y., & Owa, K. (2005). Urban–rural temperature differences in coastal cities: Influence of rural sites. *International Journal of Climatology: A Journal of the Royal Meteorological Society*, *25*(6), 811–820. https://doi.org/10.1002/joc.1180

Saleh, B., & Al Rawashdeh, S. (2007). Study of urban expansion in Jordanian cities using GIS and remoth sensing. *International Journal of Applied Science and Engineering*, *5*(1), 41–52.

Schatz, J., & Kucharik, C. (2014). Seasonality of the urban heat island effect in Madison, Wisconsin. *Journal of Applied Meteorology and Climatology*, *53*(10), 2371–2386. https://doi.org/10.1175/JAMC-D-14-0107.1

Sharma, R., & Joshi, P. K. (2015). The changing urban landscape and its impact on local environment in an Indian megacity: The case of Delhi. In *Urban development challenges, risks and resilience in Asian mega cities* (pp. 61–81). Springer. https://doi.org/10.1007/978-4-431-55043-3_4

Si, M., Li, Z.-L., Nerry, F., Tang, B.-H., Leng, P., Wu, H., Zhang, X., & Shang, G. (2022). Spatiotemporal pattern and long-term trend of global surface urban heat islands characterized by dynamic urban-extent method and MODIS data. *ISPRS Journal of Photogrammetry and Remote Sensing*, *183*, 321–335. https://doi.org/10.1016/j.isprsjprs.2021.11.017

Sobrino, J. A., Oltra-Carrió, R., Jiménez-Muñoz, J. C., Julien, Y., Soria, G., Franch, B., & Mattar, C. (2012). Emissivity mapping over urban areas using a classification-based approach: Application to the Dual-use European Security IR Experiment (DESIREX). *International Journal of Applied Earth Observation and Geoinformation*, *18*, 141–147. https://doi.org/10.1016/j.jag.2012.01.022

Strong, C., Fuentes, J. D., Davis, R. E., & Bottenheim, J. W. (2002). Thermodynamic attributes of Arctic boundary layer ozone depletion. *Atmospheric Environment*, *36*(15–16), 2641–2652. https://doi.org/10.1016/S1352-2310(97)00177-5

Su, W., Gu, C., & Yang, G. (2010). Assessing the impact of land use/land cover on urban heat island pattern in Nanjing City, China. *Journal of Urban Planning and Development*, *136*(4), 365–372. https://doi.org/10.1061/(ASCE)UP.1943-5444.0000033

Tan, M., & Li, X. (2015). Quantifying the effects of settlement size on urban heat islands in fairly uniform geographic areas. *Habitat International*, *49*, 100–106. https://doi.org/10.1016/j.habitatint.2015.05.013

United Nations, & Department of Economic and Social Affairs. (2015). *Transforming our world: The 2030 agenda for sustainable development*. https://sdgs.un.org/2030agenda

U.S. Environmental Protection Agency. (2008). *Reducing urban heat islands: Compendium of strategies. Draft.* https://www.epa.gov/heat-islands/heat-island-compendium

Voogt, J. A., & Oke, T. R. (2003). Thermal remote sensing of urban climates. *Remote Sensing of Environment*, *86*(3), 370–384. https://doi.org/10.1016/S0034-4257(03)00079-8

Wan, Z. (2008). New refinements and validation of the MODIS land-surface temperature/emissivity products. *Remote Sensing of Environment*, *112*(1), 59–74. https://doi.org/10.1016/j.rse.2013.08.027

Weng, Q. (2001). A remote sensing? GIS evaluation of urban expansion and its impact on surface temperature in the Zhujiang Delta, China. *International Journal of Remote Sensing*, *22*(10), 1999–2014. https://doi.org/10.1080/01431160118847

Yao, R., Wang, L., Huang, X., Chen, J., Li, J., & Niu, Z. (2018a). Less sensitive of urban surface to climate variability than rural in Northern China. *Science of the Total Environment*, *628*, 650–660. https://doi.org/10.1016/j.scitotenv.2018.02.087

Yao, R., Wang, L., Huang, X., Niu, Y., Chen, Y., & Niu, Z. (2018b). The influence of different data and method on estimating the

surface urban heat island intensity. *Ecological Indicators*, *89*, 45–55. https://doi.org/10.1016/j.ecolind.2018.01.044

Yohannes, H., Soromessa, T., Argaw, M., & Dewan, A. (2021). Spatio-temporal changes in habitat quality and linkage with landscape characteristics in the Beressa watershed, Blue Nile basin of Ethiopian highlands. *Journal of Environmental Management*, *281*, 111885. https://doi.org/10.1016/j.jenvman.2020.111885

Yuan, F., & Bauer, M. E. (2007). Comparison of impervious surface area and normalized difference vegetation index as indicators of surface urban heat island effects in Landsat imagery. *Remote Sensing of Environment*, *106*(3), 375–386. https://doi.org/10.1016/j.rse.2006.09.003

Zhao, J., Zhao, X., Liang, S., Zhou, T., Du, X., Xu, P., & Wu, D. (2020). Assessing the thermal contributions of urban land cover types. *Landscape and Urban Planning*, *204*, 103927. https://doi.org/10.1016/j.landurbplan.2020.103927

Zhou, D., Xiao, J., Bonafoni, S., Berger, C., Deilami, K., Zhou, Y., Frolking, S., Yao, R., Qiao, Z., & Sobrino, J. A. (2019). Satellite remote sensing of surface urban heat islands: Progress, challenges, and perspectives. *Remote Sensing*, *11*(1), 48. https://doi.org/10.3390/rs11010048

Zhou, D., Zhao, S., Liu, S., Zhang, L., & Zhu, C. (2014). Surface urban heat island in China's 32 major cities: Spatial patterns and drivers. *Remote Sensing of Environment*, *152*, 51–61. https://doi.org/10.1016/j.rse.2014.05.017

Zhou, D., Zhao, S., Zhang, L., & Liu, S. (2016). Remotely sensed assessment of urbanization effects on vegetation phenology in China's 32 major cities. *Remote Sensing of Environment*, *176*, 272–281. https://doi.org/10.1016/j.rse.2016.02.010